Multimed Tools Appl
DOI 10.1007/s11042-017-4474-7

Computer-aided detection and quantification in glistenings on intra-ocular lenses

Parisut Jitpakdee[1] · **Bunyarit Uyyanonvara**[1]

Received: 15 September 2016 / Revised: 26 December 2016 / Accepted: 1 February 2017

Abstract The artificial intraocular lens (IOL) is inserted to replaced the crystalline lens of the human eye after cataract surgery or refraction clear lens extraction. When the IOL, is in an aquatic environment, glistenings, which are liquid-filled microvacuoles, can be discriminated from normal state. Automatic detection of glistenings is a new problem, they have tiny sizes, sometimes have low contrast and also similar with the lens background. In this paper, the candidate glistenings are automatically detected by mathematic morphology method and fine segmented using the classifiers, we used k-nearest neighbor (kNN) and Naïve Bayes for comparing the results. The detected glistenings are validated by object-based with ophthalmologists hand-drawn ground-truth. The result shows that classification can improve the performance of glistenings detection better than using only morphology method. The proposed software was developed for creating an effective automatic glistenings detection and quantification with a user-friendly Graphical User Interface,reliable results. Thus this computer-aid tool will help the researcher analyze the experiment results to better understand glistenings characteristic that have an effect on vary conditions.

Keywords Medical image processing · Computer-aided detection · Feature extraction · Classification

1 Introduction

In pathological conditions such as cataract, the natural lens of a human eye is being replaced by an artificial intraocular lens (IOL) inserted in the capsular bag [3]. Glistenings is a phenomenon of liquid-filled microvacuoles in implanted lenses and reduce clarity of lens have an affect on

✉ Parisut Jitpakdee
parisut@gmail.com

Bunyarit Uyyanonvara
bunyarit@siit.tu.ac.th

[1] School of Information, Computer, and Communication Technology, Sirindhorn International Institute of Technology, Thammasat University, 131 Moo 5, Bangkadi, Pathum Thani 12000, Thailand

Published online: 14 February 2017

optical function [17]. In many studies, glistenings were found after implantation although the times of onset were different [14, 18, 25, 28]. The earliest onset time of glistenings is a week postoperative. In some patients, glistenings could not be found up to 6 months after implantation [28]. The visual effects of glistenings due to forward light scatter have been evaluated in numerous studies [14, 19, 27]. There are many determinants influencing glistenings formation, such as temperature changing, IOL material, IOL manufacturing and packaging technique and IOL packaging [12, 14, 16, 17, 20, 25]. Glistenings observing was reported first time in [14]. Glistenings are seen as outstanding dots within the IOL lens [12]. Many research studies show the glistenings formation in different ways [12–14, 16–18, 28]. The work of Werner [17] described how to grade the glistenings by using the density. The grades were 0 for no glistenings; 1 for up to 50/mm^3; 2 for up to 100/mm^3; and 3 for up to 200/mm^3.

In medical computer-aid detection system assist doctors in analysis and interpretation images. Application [4] is proposed as the automated tool for nuclei detection in digital microscopic images. Software for detection of diabetic retinopathy on non-dilated retinal image prensented in [6]. They use mathematical morphological process for detection. Software, CellProfiler is the image analysis software for identifying and quantifying cell phenotypes [5]. Glistenings detection with simple image processing methodology were presented in our previous work [15]. The prototype software can detect the glistenings using the simple morphological image segmentation method and with semi-automatic process however the user needs to adjust some parameters of each IOL image.

This paper presents a fully-automatic method for accurate glistenings detection using Pattern recognition and classification method. Pattern recognition and classifications are essential in many medical applications such as cancer detection. Cancer diagnosis using image processing and pattern recognition are presented in [1]. Blobs detection, the important problem in medical image processing uses techniques similar to those implemented for glistenings detection. There are many research publications that employ feature extraction and classification method, such as exudate detec-tion and microaneurysms in retinal images [22–24]. In [26] detected candidate lesion regions by adap-tive intensity thresholding and used and a neural network for classification. Many techniques such as using the Gabor wavelets and the circle Hough transform have been used to detect circles. A. Rhodes and L. Bai. [21] proposed a “Gabor Annulus” technique, based on the principles of Gabor wavelets, for the purpose of circular feature detection. Texture segmentation using circular Gabor filters (CGF) are proposed in [29].

In this study, we detected the candidate glistenings by using a set of mathematical morphology. In order to increase the accuracy and performance of glistenings detection, classifier is used. We compared the performance of k-Nearest Classifier and Naive Bayes classifier by evaluating average sensitivity, specificity, precision and accuracy, against ophthalmologist’s hand-drawn ground-truth.

The paper is organized as follows. Section 2 presented our methodology candidate glistenings detection, feature extraction and glistenings classification. The experimental results are showed in Section 3. Section 4 describes the quantification of glistenings and shows the example screen of software. Finally, section 5 is a conclusion of this study.

2 Methodology

We obtained 27 digital Intraocular Lens Glistenings images captured with a digital Nikon FS-2 photo slit-lamp. The images taken for in vitro experiment from the Applied Vision Research Centre, School of Health Sciences, City University London. The images are downsized from

3216 × 2136 to 750 × 499. Examples of IOL images are shown in Fig. 1. Examples of glistenings and non-glistenings are presented in Fig. 2. Even though, the number of images in the experiment seems small, but our experiments are blob-based detection not image-based classification. Number of blobs on images are big enough for training and testing as shown in Table 1.

The overall process is shown in Fig. 3. First the RGB IOL image is converted to the grayscale image by using a red band. The candidate glistenings then are detected using the procedure described in Section 2.1. Next step, the important features are extracted from image collection and then glistening classification are performed.

The following section describes the detail of processes after converting to grayscale.

2.1 Glistening candidates extraction

In our approach, the glistening candidates are extracted by using a set of mathematical morphology. First, glistenings' edges are detected by Sobel operator from red band IOL images [7]. The Sobel operator performs a 2-D spatial gradient measurement on an image and underlines areas of high spatial frequency that correspond to edges [11]. In our method, we used both horizontal and vertical direction of detection for the Sobel method and used the sensitivity threshold 0.02 to ignore all weak edges.

A dilation operation is then used for joining the sub-sequence lines. Dilation will fill all close regions with white color. The example images of close-up glistening candidate detection method are shown in Fig. 4.

The candidate glistenings blobs are detected and classified into glistenings and non-glisteings by the opthalmologist which will be used as groundtruths. There are 6830 glistenings and 2355 non-glistenings from 27 images as shown in Table 1.

2.2 Feature extraction

In this stage, we proposed 20 features to distinguish glistening from non-glistening objects. All 20 features are listed in this section with a brief description of each feature as follows: Color gives influential information for object recognition and in the case of glistenings, their colors are different from background, so we used the mean intensity of red, green and blue as features 1, 2 and 3. Most of glistenings are like droplets but they are not so smooth as the background the standard deviation of intensity would distinguish the glistenings from the background. The standard deviation of the 3 channels are also chosen for features 4,5 and 6. Most of noise or non-glistenings are small islands appearing around the border of the lens, so the distance between the candidate blob and lens' centroid and area are used for feature 7 and 8. Glistening is a round shape object, so the shape features; Eccentricity, EquivDiameter, Perimeter, Compactness, and Solidity are used to classify line object and noise from glistenings and they are feature 9,10,11,12 and 13. Laplacian of Gaussian is one of general scale invariant region detection

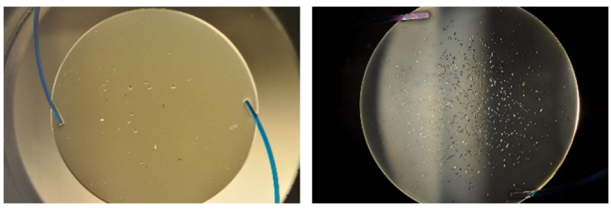

Fig. 1 Sample of IOL images

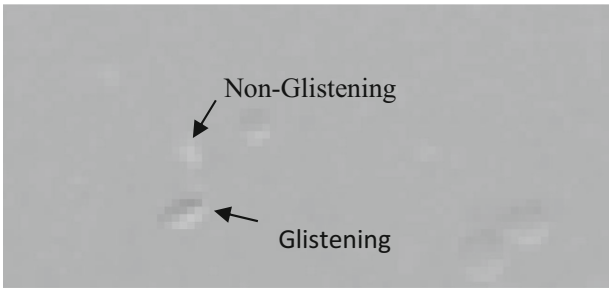

Fig. 2 Glistening vs. Non-Glistening object

and we use it as the feature number 14. Gabor filter is also used generally for texture analysis, and we thought the texture of the glistenings are so different from its background. So we used 6 orientation of the Gabor filter for our feature number 16–20.

List of features:

1–3) The mean intensity in the image, red, blue, green channel.
4–6) The standard deviation of intensity in the red, blue, and green band image.
7) Distance: the distance between Centroid of the lens and glistening candidate.
8) Area: the number of pixels in the glistening candidate boundary.
9) Eccentricity: the ratio of the distance between the foci of the ellipse and its major axis length.
10) EquivDiameter: the diameter of a circle having the same area as the glistening candidate region.
11) Perimeter: the total number of pixels on the boundary of each glistening candidate region in the image.
12) Compactness: the variance of the radial distance of the object"s pixels from the centroid divided by the area.
13) Solidity: the ratio of the pixels in the convex hull that are also in the object.
14) LoG: the average of pixel's intensity value in red band image filtered with Laplacian of Gaussian method. We used filter size =3 with standard deviation sigma =0.25
15–20) two dimensional Gabor filtered in 6 different orientations.

Table 1 Number of glistenings and non-glistenings in 27 image

Image	Glisteings	Non-Glistenings	Image	Glisteings	Non-Glistenings
1	624	245	14	204	32
2	570	205	15	236	3
3	636	476	16	136	54
4	228	89	17	274	44
5	134	30	18	241	34
6	374	287	19	259	13
7	231	210	20	331	118
8	120	8	21	382	11
9	191	52	22	344	50
10	230	18	23	66	16
11	373	47	24	26	35
12	197	104	25	48	60
13	120	34	26	91	54
14	204	32	27	164	26
15	236	3	Total	6830	2355

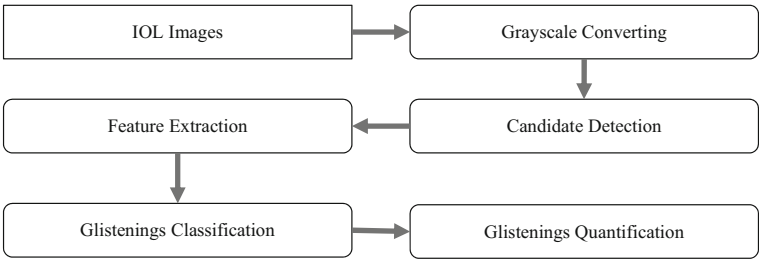

Fig. 3 The proposed flow chart of an automated Glistenings Detector System

A two-dimensional Gabor filter is a Gaussian kernel function modulated by a complex sinusoidal plane wave, defined as follows [21]:

$$G(x,y) = \frac{f^2}{\pi\gamma\mu} exp\left(-\frac{x'^2 + y^2 y'^2}{2\sigma^2}\right) exp\left(j2\pi f x' + \varnothing\right) \tag{1}$$

$$x' = xcos\theta + ysin\theta \tag{2}$$

$$y' = -xsin\theta + ycos\theta \tag{3}$$

Where f is the frequency of the sinusoidal factor, θ is the orientation of the normal to the parallel stripes of a Gabor function, ϕ is the phase offset, σ is the standard deviation and γ is the spatial aspect ratio.

In this paper, we used θ = 0, π/6, 2π/6, 3π/6, 4π/6, and 5π/6.

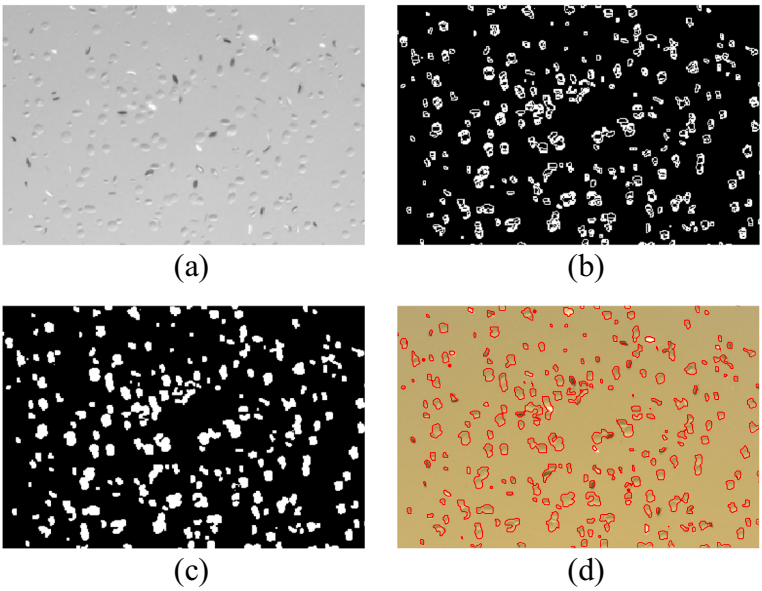

Fig. 4 Candidate glistenings detection. **a** Gray-scale image. **b** Edge detection and dilation. **c** Hole Filling. **d** Candidate glistenings Edges

2.3 Glistenings classification

A fine segmentation, glistenings classification is the final stage where true glistenings are detected from all candidate regions. The feature vectors of candidate glistenings are classified into 2 classes: 'glistenings' and 'non-glistenings' by 3 methods for comparison k-NN classifier and Naive Bayes classifier.

a. *k-Nearest Neighbor Classification*

The k-nearest neighbors (k-NN) algorithm is one of familiar machine learning method. This classification algorithm finds nearest neighbors of a test object. The object will be assigned to the class by majority voting amongst its k nearest neighbors measured by a distance function. [2]. In this study, we used k = 5 and measure the distance with the Euclidean distance [8].

b. *Naive Bayes Classifi*cation

Naive Bayes classifiers apply Bayes" theorem to classify by assumes that the feature of a class is unrelated to any other feature [9]. Maximum a posteriori or *MAP* decision rule is combined with independent feature probability model in Naive Bayes classifier, the classify function assigns a class label $\widehat{y} = C_i$ defined as follows:

$$\widehat{y} = \underset{i\in\{1,\ldots,k\}}{\operatorname{argmax}} P(C_i)\prod_{j=1}^{n} P\left(x_j|C_i\right) \tag{4}$$

Where $P(x_j \mid C_i)$ is the likelihood of feature vector x_j given class C_i, $P(C_i)$ is the prior probability of class C_i, k is the number of class and n is the number of features or size of data vector.

Before classification, all training data are normalize by min-max-scaling.

$$x^{'} = \frac{x - min(x)}{max(x) - min(x)} \tag{5}$$

where x is an original value, x" is the normalized value.

3 Validation

Dataset of 27 IOL images are performed processing on an Intel(r) Core™ i7-4510 U CPU @ 2.00GHz 2.60GHz using the MATLAB program version R2012a. We evaluated using 3-fold Cross Validation Testing, creates a 3-fold partition of the dataset. For each of experiments, we used 2 folds for training (18 images) and the rest one for testing (9 images).

For each image in the training set and testing set, we extracted the features for every candidate glistenings.

Detected glistenings are compared with the ground-truth images drew by the ophthalmologists for verification. Precision, Recall, and F-Measure are chosen as the measurements of the accuracy of the algorithms. Precision measure the exactness of the classifiers while recall measures the completeness of the classifiers. The F-measure score shows the balance between the precision and the recall. All measures can be calculated from true positive (TP) rate, the

false positive (FP) rate, the false negative (FN) rate, and the true negative (TN) rate. From these quantities, The precision is computed by TP/(TP + FP), recall is calculated by TP/(TP + FN), where TP is true positive rate, FP is the false positive rate and FN is the false negative rate. F-Measure is calculated by

$$F\_Measure = 2\,\frac{Precision \times Recall}{Precision + Recall} \tag{6}$$

Non-classifier (using only mathematical morphology) K-Nearest Neighbor (KNN) and Naïve Bayes classifier are selected for comparison of the performance. The result of classification is shown in Table 2. The result shows that F-measure value from kNN classifier better than Naïve Bayes classifier, so in our software we use kNN as the classifier.

The result of using only mathematical morphology, there are some false glistenings detection appears. This experiment has shown that the proposed method could detect those misclassified glistenings. Fig. 5. shows the classification result on IOL image from Naïve Bayes classifier. The true glistenings (TP) are shown in the green edge. Blue edge objects are the candidate glistenings the classified correctly to not glistenings class (TN), while the red edge objects are wrong classified as glistenings (FP). Missing glistenings (FN) are in the black edge.

Table 2 Object-based classification validation result

Image	Precision			Recall			F-measure		
	Non-Classifier	Naïve Bayes	kNN	Non-Classifier	Naïve Bayes	kNN	Non-Classifier	Naïve Bayes	kNN
1	0.7031	0.7181	0.7171	0.7977	1.0000	0.9952	0.7474	0.8359	0.8336
2	0.7252	0.7355	0.7399	0.8110	1.0000	0.9930	0.7657	0.8476	0.8479
3	0.4236	0.9091	0.5398	0.5822	0.0157	0.8097	0.4904	0.0309	0.6478
4	0.6498	0.9524	0.7143	0.7658	0.2632	0.9649	0.7031	0.4124	0.8209
5	0.7500	0.8199	0.8160	0.6649	0.9851	0.9925	0.7049	0.8949	0.8956
6	0.4947	0.5658	0.5658	0.6756	1.0000	1.0000	0.5712	0.7227	0.7227
7	0.5011	0.8133	0.5197	0.9485	0.5281	0.9697	0.6558	0.6404	0.6767
8	0.9141	0.9286	0.9370	0.5493	0.2167	0.9917	0.6862	0.3514	0.9636
9	0.7654	0.7860	0.7915	0.8341	1.0000	0.9738	0.7983	0.8802	0.8732
10	0.8952	1.0000	0.9234	0.8506	0.0652	0.9435	0.8723	0.1224	0.9333
11	0.8119	0.8961	0.8974	0.7949	0.9946	0.9142	0.8033	0.9428	0.9057
12	0.5748	0.9111	0.6508	0.9010	0.2081	0.9746	0.7018	0.3388	0.7805
13	0.6623	0.7792	0.7792	0.7669	1.0000	1.0000	0.7108	0.8759	0.8759
14	0.7500	0.8777	0.8603	0.8389	0.9853	0.9657	0.7919	0.9284	0.9099
15	0.9582	0.9874	0.9874	0.6156	1.0000	1.0000	0.7496	0.9937	0.9937
16	0.6368	0.7158	0.7158	0.9453	1.0000	1.0000	0.7610	0.8344	0.8344
17	0.7075	0.8616	0.8616	0.7550	1.0000	1.0000	0.7305	0.9257	0.9257
18	0.8255	0.8764	0.8764	0.9538	1.0000	1.0000	0.8850	0.9341	0.9341
19	0.8971	0.9522	0.9522	0.8971	1.0000	1.0000	0.8971	0.9755	0.9755
20	0.6793	0.9773	0.7449	0.8944	0.5196	0.9879	0.7722	0.6785	0.8494
21	0.9644	0.9720	0.9720	0.7550	1.0000	1.0000	0.8469	0.9858	0.9858
22	0.8401	1.0000	0.8646	0.7995	0.4477	0.9099	0.8193	0.6185	0.8867
23	0.4512	0.8049	0.8049	0.8043	1.0000	1.0000	0.5781	0.8919	0.8919
24	0.3443	0.5556	0.4310	0.9130	0.1923	0.9615	0.5000	0.2857	0.5952
25	0.4074	0.4444	0.4444	0.7458	1.0000	1.0000	0.5269	0.6154	0.6154
26	0.2414	0.6250	0.6276	0.7143	0.9890	1.0000	0.3608	0.7660	0.7712
27	0.8053	0.8670	0.8571	0.4069	0.9939	0.9146	0.5406	0.9261	0.8850
Total	0.6807	0.8271	0.7627	0.7771	0.7557	0.9727	0.7026	0.7132	0.8456

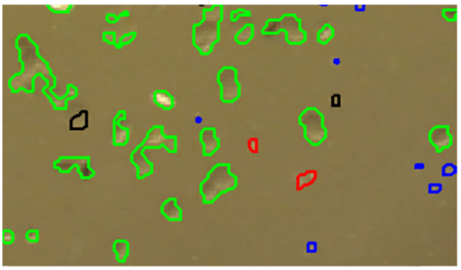

Fig. 5 Glistenings detection result

4 Glistening quantification software

This software was a collaboration of Kingston University, UK and SIIT, Thammasat University, Thailand, developed for creating an effective glistenings detection and quantification with a user-friendly Graphical User Interface (GUI). The detection and quantification steps proceed as follows:

1) The user selects the image file loaded to the software's interface as shown on Fig. 6. Then the lens size is selected, 6 mm or 7 mm optic diameter.
2) The lens bouldery is defined by choosing from a pre - hand drawn lens masks or automatic generating by just marking 5 different points on the IOL's edge. The software will find the best-fit circle. (Fig. 7).

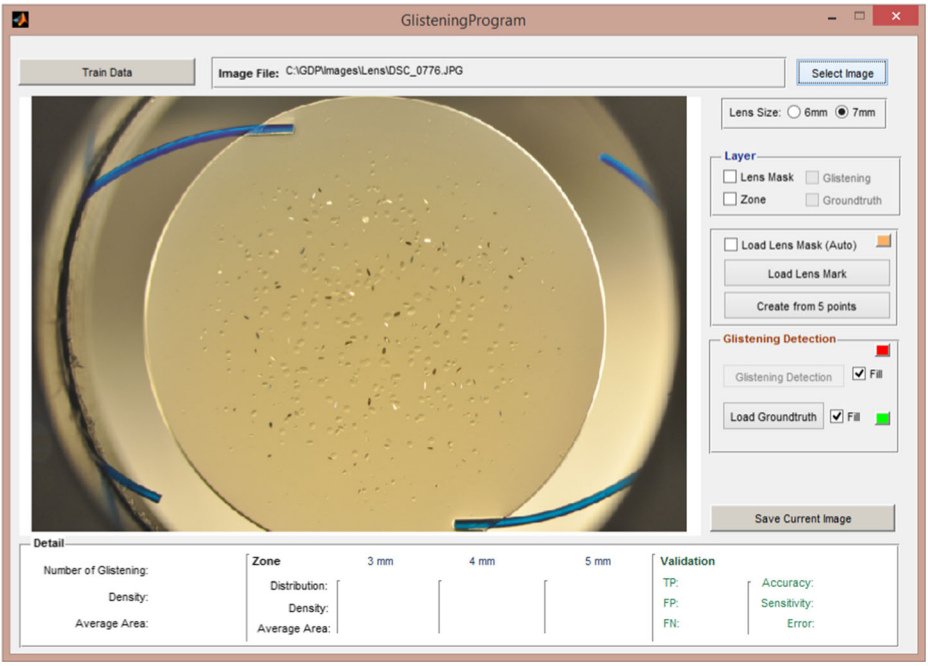

Fig. 6 Graphical user interface for glistenings detection software

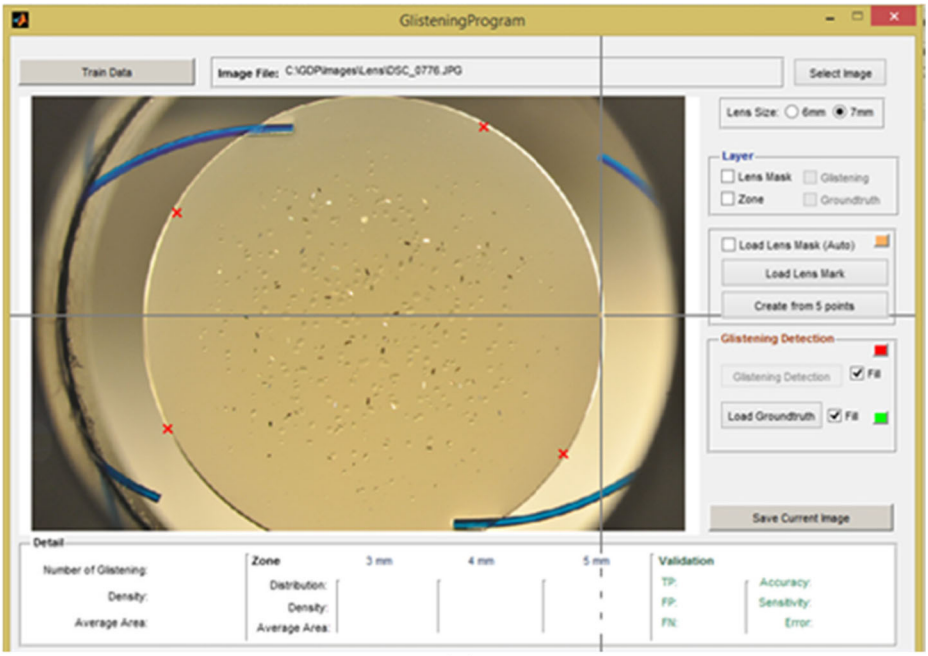

(a)

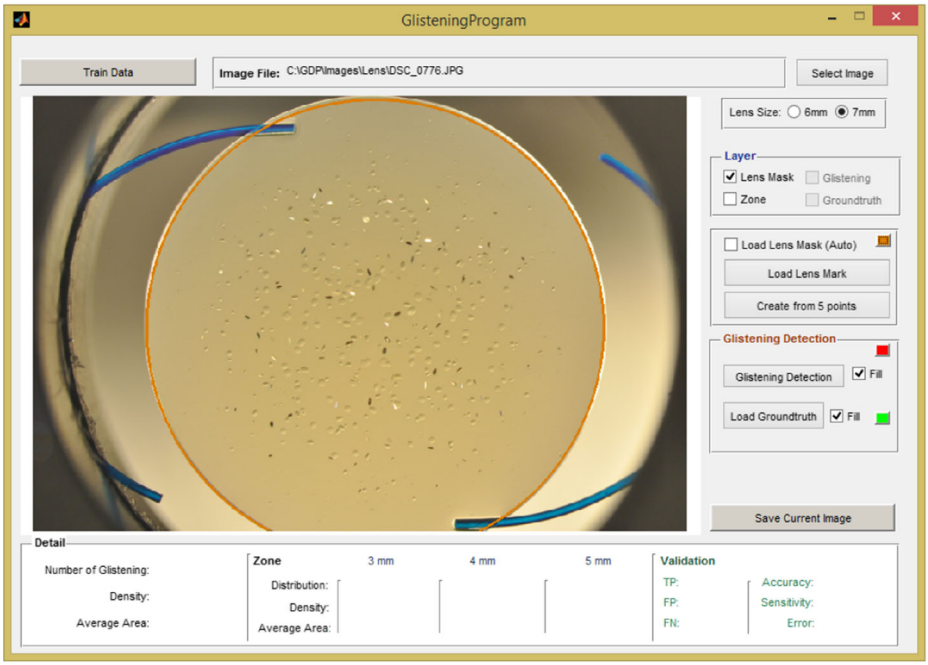

(b)

Fig. 7 **a** 5 different points manually marked on the IOL's edge. **b** A best fit Lens bouldery generated

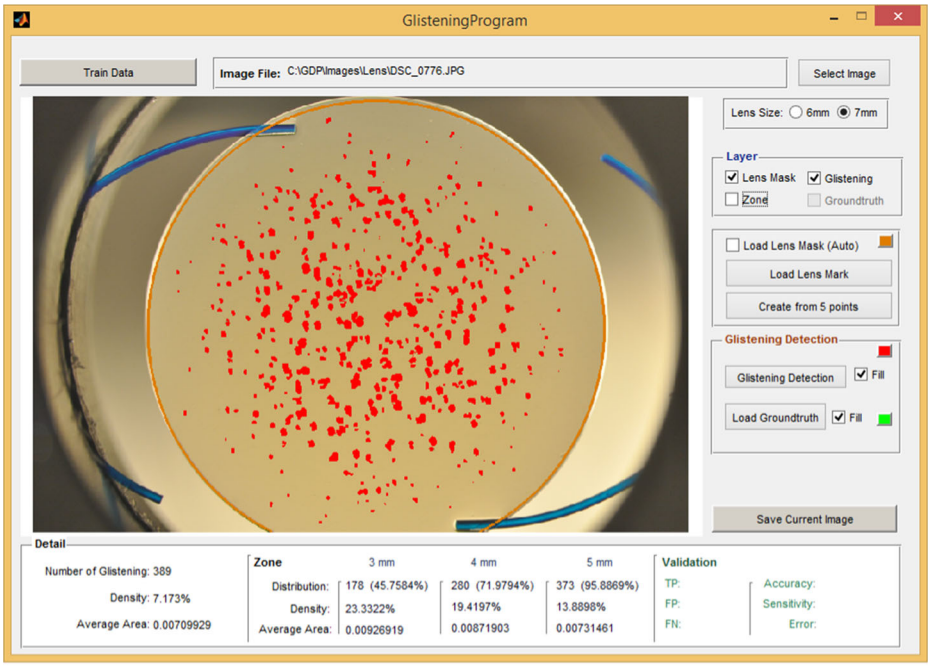

(a)

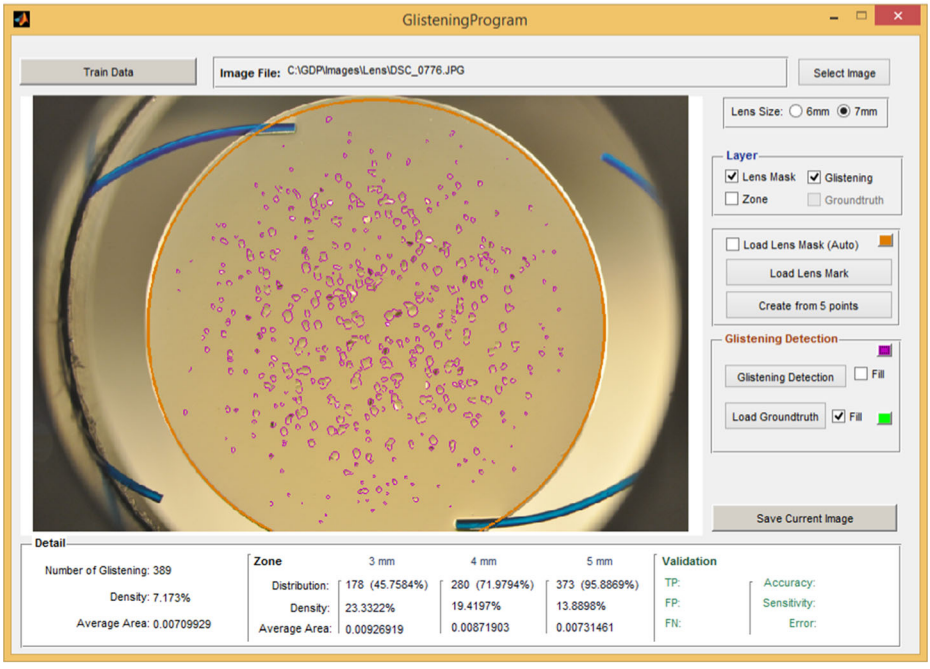

(b)

Fig. 8 Output from the Glistenings Detection Program (**a**) filled glistenings (**b**) glistenings edges with selected color

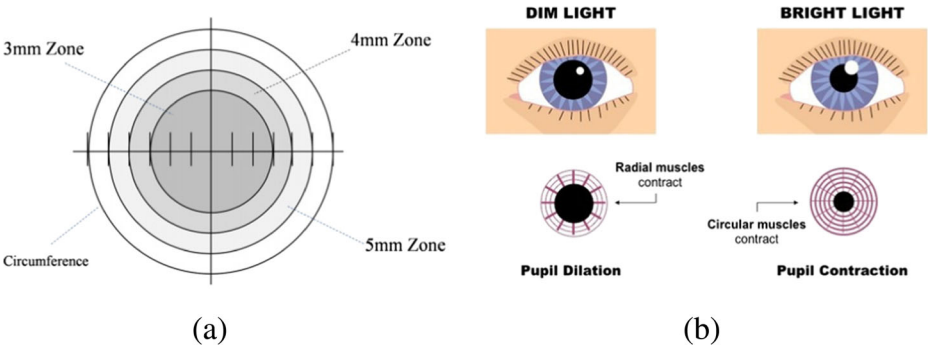

Fig. 9 **a** Lens zones for a 6 mm optic diameter IOL (**b**) the pupil reflex [10]

3) When glistening detection and classification by k-Nearest Neighbor method, the previously described methodology finished, the detected glistenings are showed on the lens image. Quantification metrics are also reported and exported to an excel file for further evaluation and analysis by the clinician. The user can select to showing the detected glistenings by filling or just the edge of glistenings and can change the color. (Fig. 8).
4) The software also show the zone of the IOL lens. Lens is divided mimic the different sizes of pupil. Glistenings are detected and quantified in divided 3 concentric zones; 3 mm, 4 mm, and 5 mm. Fig. 9 shows the zoning system described in this paper and Fig. 10 shows the zoning on the screen.

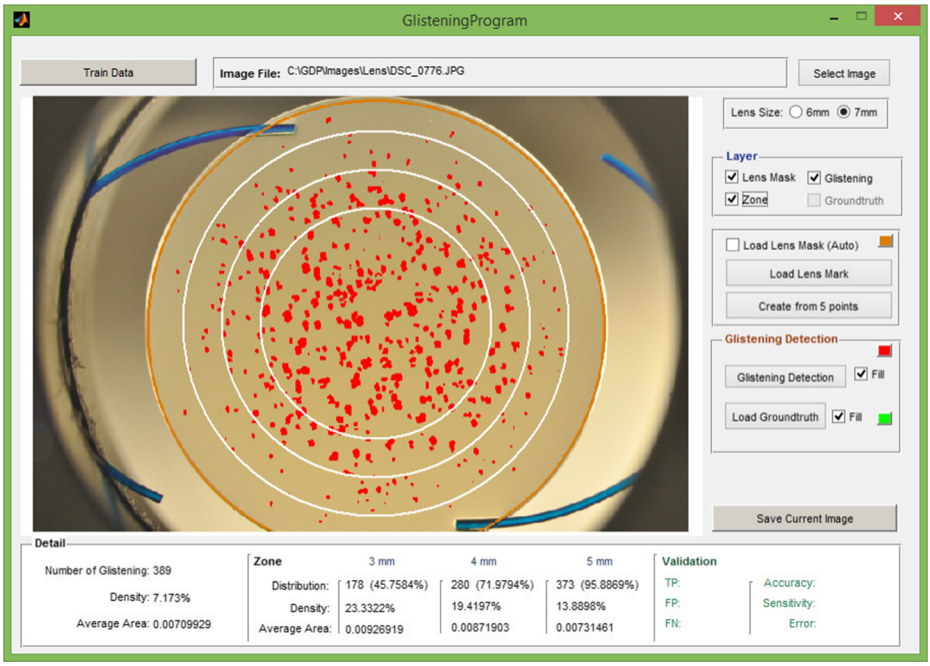

Fig. 10 **a** Lens divided to 3 zones on the screen

5) The Quantification information, density (Eq. 7), distribution (Eq. 8) and average area (Eq. 9), were calculated for four different optical zones: the whole lens and 3 mm, 4 mm and 5 mm diameter and showed at the bottom of the interface.

$$Density = \frac{sum\ of\ all\ glistenings' areas\ included\ in zone}{zone's\ area} \times 100\% \tag{7}$$

$$Distribution = \frac{number\ of\ glistetings\ in\ optical \text{zone}}{number\ of\ glistenings\ in\ whole\ IOL} \times 100\% \tag{8}$$

$$Average\ Area = \frac{sum\ of\ all\ glistenings' areas\ included\ in\ zone}{number\ of\ glistetings\ in\ \ zone} \times 100\% \tag{9}$$

5 Conclusion

This paper proposed a Glistenings Detection and quantification software help the clinician to analysis the experimental result to better understand the effect of glistenings with parameters and conditions. The proposed glistenings detection based on a hybrid approach of two techniques, mathematical morphology and fine segmentation using two classifiers for comparing the results. The twenty features are proposed based on characteristics of glistenings. The results have shown that the precision, recall, and F-measure value increase after fine segmentation using both k-NN and Naive Bayes classifier.

For future work, we will focus on the problem of overlapping glistenings and improve the fine segmentation performance by selecting the features before the classification process which can help for better quatification and grading of glistenings.

Acknowledgements This research is funded by the National Research University Project of Thailand Office of Higher Education Commission (Thammasat University). We would like to thank the Applied Vision Research Centre, School of Health Sciences, City University London, for the IOL images and ground truth data.

References

1. Abarghouei A, Ghanizadeh A, Sinaie S, Shamsuddin S (2009) A Survey of Pattern Recognition Applications in Cancer Diagnosis. Proc. International Conference of Soft Computing and Pattern Recognition, pp 448–453
2. Altman NS (1992) An introduction to kernel and nearest-neighbor nonparametric regression. Am Stat 46(3): 175–185

3. Bellucci R (2013) An introduction to intraocular lenses: material, optics, haptics, design and aberration
4. Byun J, Verardo MR, Sumengen B, Lewis GP, Manjunath BS, Fisher SK (2006) Automated tool for nuclei detection in digital microscopic images: application to retinal images. Mol Vis 12:949–960
5. Carpenter AE, Jones TR, Lamprecht MR, Clarke C, Kang IH, Friman O, Guertin DA, Chang JH, Lindquist RA, Moffat J, Golland P, Sabatini DM (2006) CellProfiler: image analysis software for identifying and quantifying cell phenotypes. Genome Biol 7(10):R100
6. Datta NS, Sarker R, Dutta HS, De M (2012) Software based automated early detection of diabetic retinopathy on non dilated retinal image through mathematical morphological process. Int J Comput Appl 60(18):20–24
7. Davies E (1990) Machine vision: theory, algorithms and practicalities, Chap. 5. Academic Press, London
8. Deza E, Deza MM (2009) Encyclopedia of distances. Springer, p 94
9. Friedman N, Geiger D, Goldszmidt M (1997) Bayesian network classifiers. Mach Learn 29:131–163
10. Gillam P (2014) How do the muscles in the iris bring about the pupil reflex?. [image] Available at: https://pmgbiology.com/tag/pupil-reflex/. Accessed 8 Feb 2017
11. Gonzalez RC, Woods RE (2002) Digital image processing, 2nd edn. Prentice Hall, Upper Saddle River
12. Gregori NZ, Spencer TS, Mamalis N, Olson RJ (2002) In vitro comparison of glistening formation among hydrophobic acrylic intraocular lenses. J Cataract Refract Surg 28(7):1262–1268
13. Gunenc U, Oner FH, Tongal S, Ferliel M (2001) Effects on visual function of glistenings and folding marks in AcrySof intraocular lenses. J Cataract Refract Surg 27(10):1611–1614
14. Hayashi K, Hirata A, Yoshida M, Yoshimura K, Hayashi H (2012) Long-term effect of surface light scattering and glistenings of intraocular lenses on visual function. Am J Ophthalmol 154(2): 240–251.e2
15. Japunya T, Jitpakdee P, Uyyanonvara B, Aimmanee P, Philippaki E, Hull C, Barman S (2014) Software for the Quantification of Glistenings in Intra-Ocular Lenses. Proceedings of the World Congress on Engineering, vol I. WCE 2014, London, 2–4 July 2014, pp 34–38
16. Kato K, Nishida M, Yamane H, Nakamae K, Tagami Y, Tetsumoto K (2001) Glistening formation in an AcrySof lens initiated by spinodal decompositionof the polymer network bytemperature change. J Cataract Refract Surg 27(9):1493–1498
17. Malley M (1995) AcrySof `glistenings' and questions of haze. Ophthalmology Times 20(18):1
18. Mamalis N (2012) Intraocular lens glistenings. J Cataract Refract Surg 38(7):1119–1120
19. Mönestam E, Behndig A, Medicinska fakulteten, Oftalmiatrik, Institutionen för klinisk vetenskap & Umeå universitet (2011) Impact on visual function from light scattering and glistenings in intraocular lenses, a long-term study. Acta Ophthalmol 89(8):724–728
20. Oshika T, Shiokawa Y, Amano S, Mitomo K (2001) Influence of glistenings on the optical quality of acrylic foldable intraocular lens. Br J Ophthalmol 85(9):1034–1037 [online]. Available: http://www.ncbi.nlm.nih.gov/pmc/articles/PMC1724105/pdf/v085p01034.pdf
21. Rhodes A, Bai L (2011) Circle Detection Using a Gabor Annulus. Proceedings of the 22nd British Machine Vision Conference, Dundee
22. Sopharak A, Dailey M, Uyyanonvara B, Barman S, Tom W, New KT, Moe YA (2010) Machine learning approach to automatic exudate detection in retinal images from diabetic patients. J Mod Opt 57(2):124–135
23. Sopharak A, Uyyanonvara B, Barman S (2012) Fine Microaneurysm Detection from Non-dilated Diabetic Retinopathy Retinal Images Using a Hybrid Approach. Dr. Akara Sopharak The 2012 International Conference of Signal and Image Engineering (ICSIE), Imperial College, London, 4–6 July 2012
24. Sopharak A, Uyyanonvara B, Barman S (2014) Comparing SVM and Naïve Bayes Classifier for Automatic Microaneurysm Detections. ICISVC 2014: International Conference on Image, Signal and Vision Computing, in Tokyo, Japan, 29–30 May 2014
25. Tognetto D, Toto L, Sanguinetti G, Ravalico G (2002) Glistenings in foldable intraocular lenses. J Cataract Refract Surg 28(7):1211–1216
26. Usher D, Dumskyj M, Himaga M et al (2004) Automated detection of diabetic retinopathy in digital retinal images: a tool for diabetic retinopathy screening. Diabet Med 21(1):84–90
27. van der Mooren M, Franssen L, Piers P (2013) Effects of glistenings in intraocular lenses. Biomedical Optics Express 4(8):1294–1304
28. Werner L (2010) Glistenings and surface light scattering in intraocular lenses. J Cataract Refract Surg 36(8): 1398–1420
29. Zhang JG, Tan T, Li M (2002) Invariant Texture Segmentation via Circular Gabor Filters. In Proceedings of the 16th IAPR International Conference on Pattern Recognition (ICPR), Quebec City, 11–15 Aug 2002, pp 901–904

Parisut Jitpakdee received the B.Sc. degree in computer science from Chiang Mai University, Thailand, in 2004 and the M.Sc. degree in information technology (information science) from King Mongkut's Institute of Technology Ladkrabang, Thailand in 2007. She is now a Ph.D. candidate student at Sirindhorn International Institute of Technology, Thammasat University, Thailand and active in a field of medical image processing.

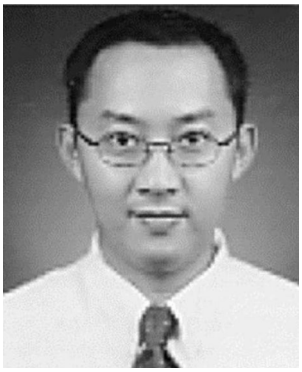

Bunyarit Uyyanonvara received the B.Sc. degree (1st Class Honors) from Prince of Songkhla University, Thailand, in 1995 and the Ph.D. degree in medical image analysis from King's College, London, U.K., in 2000. He is now an Associate Professor at Sirindhorn International Institute of Technology, Thammasat University, Thailand and active in a field of medical image processing.